SUPPLEMENTARY INFORMATION

The same pocket in menin binds both MLL and JunD, but oppositely regulates transcription

Jing Huang, Buddha Gurung, Bingbing Wan, Ke Wan, Xianxin Hua, and Ming Lei

Supplementary Text

Crystallization of menin and the menin-MLL1$_{MBM}$ complex

Because there were no recognizable domains in menin[1], to begin to structurally characterize this protein and its interaction with MLL1, we initially expressed and purified full-length human menin. However, full-length protein was unstable by itself and prone to be degraded (data not shown). Multiple sequence alignment of menin proteins from different organisms clearly revealed a less conserved region, which is dominated by stretches of charged residues and hydrophilic amino acids that favor disordered structures (e.g., glycine, proline, and serine) (Supplementary Fig. 3a). This region in human menin consists of residues 460-550 (Supplementary Fig. 3a). Protein sequence analysis by various programs, including FoldIndex program[2], predicted that human menin$_{460-540}$ is not folded (Supplementary Fig. 3b). By contrast, except for the termini and two short segments, the remainder of menin was predicted to be folded (Supplementary Fig. 3b). Notably, a strong yeast-two-hybrid interaction was detected between the two regions that are separated by menin$_{460-540}$ (Supplementary Fig. 3c). Thus, these analyses suggested

that menin adopts a compact fold with a large 80-residue unstructured loop in the middle of the protein (Supplementary Fig. 3a). For structural studies, a panel of menin constructs with different deletions inside menin$_{460\text{-}540}$ were prepared and used in crystallization trials (data not shown). After extensive screening, one such deletion mutant menin$_{\Delta 460\text{-}519}$ yielded proteins with good quality and generated crystals suitable for structural determination.

Structural architecture of menin

Although primary sequence analysis failed to identify any known protein motif in menin, strikingly, an unbiased search using Dali[3] revealed unequivocal structural resemblance of individual menin domains with well-characterized protein motifs in the database (Supplementary Fig. 4a). The structure of menin thumb domain is most similar to the transglutaminase-like fold of peptide-N-glycanase (PNGase), which characterizes the transglutaminase superfamily[4]. The transglutaminase-fold of PNGase can be superimposed onto the thumb domain with a root-mean-square deviation (rmsd) of ~3.6 Å in the positions of 92 equivalent Cα atoms (Supplementary Fig. 4b). However, the menin thumb domain lacks the Cys-His-Asp catalytic triad characteristic of the transglutaminase family[4] (Supplementary Fig. 4c). The corresponding residues (Ser$_{154}$-His$_{181}$-Glu$_{195}$) in the thumb domain are buried inside the structure by a large loop that is absent in PNGase (Supplementary Fig. 4c). Furthermore, when the structure of menin-MLL1$_{MBM}$ is superimposed with that of PNGase complexed with the substrate

peptide[5], $MLL1_{MBM}$ and the substrate peptide occupy the same binding site on menin and PNGase (Supplementary Fig. 4b). Therefore, we conclude that the thumb domain of menin is a transglutaminase-like protein-protein interaction module that lacks enzymatic activity.

The palm domain of menin contains a meander of eight α helices that are arranged in a head-to-tail manner and closely resembles the two TPR (tetratrico-peptide repeat) domains of Hop (Hop_{TPR1} and Hop_{TPR2A}) with rmsd values of 2.7 Å and 2.6 Å, respectively (Supplementary Figs. 4d and 4e). TPR domains normally consist of three or more TPR motifs, which are highly degenerate 34-amino-acid repeats[6]. Similar to Hop_{TPR1} and Hop_{TPR2A}, $menin_{palm}$ consists of three TPR motifs and a C-terminal helix, which is also an integral part of the Hop TPR domains (Supplementary Fig. 4f). Notably, the first TPR motif of the palm domain contains a putative nuclear receptor-binding motif – LLWLL[7] (Supplementary Fig. 4f), which was proposed to mediate the interaction with estrogen receptor-α (ERα)[8]. However, our crystal structures showed that these leucine residues have structural stabilizing roles in a buried environment (Supplementary Fig. 4g), suggesting that the LLWLL sequence of menin is unlikely involved in the interactions with ERα and other nuclear receptors. TPR domains serve as protein-protein interaction modules[6]. The regular TPR helical meanders form cradle-shaped grooves that accommodate peptides in an extended conformation[9] (Supplementary Figs. 4d and 4e). In contrast, both the palm and the thumb domains in menin are required for $MLL1_{MBM}$ binding. They constitute a palm-like cavity that forces the $MLL1_{MBM}$ peptide to adopt a

highly coiled conformation (Fig. 1d).

A comparison of NTD of menin with the β-hairpin domains of nucleotide excision repair protein XPA[10] reveals an intriguing similarity (Supplementary Fig. 4h). Although structure superposition shows poor alignment, they share a common topology. The primary feature of these domains is a large β-hairpin supported by a helical bundle (Supplementary Fig. 4h). The concaved surface of the helical bundle in XPA mediates interactions with DNA molecules[10]. In contrast, the same surface on $menin_{NTD}$ binds one end of the palm domain and is essential for protein stability (Fig. 1d).

Unlike the other three domains, the fingers domain of menin has no homology with any known motif in the database. It is composed of two sets of α/β motifs ($menin_{402-459}$ and $menin_{548-581}$), which are closely associated in 3D structure but separated in primary sequence by a large 90-residue loop (Supplementary Fig. 4i). The association between the two α/β motifs is mediated by extensive hydrophobic contacts, a parallel β-strand pair as well as several clusters of electrostatic interactions Supplementary Fig. 4i). This interface between the two α/β motifs is essential for menin integrity as deletion of the C-terminal α/β motif greatly reduced the stability of the protein as attempts to express and purify $menin_{1-460}$ only yielded insoluble and aggregate products (data not shown). The importance of this region of menin is further highlighted by the identification of many *MEN1* frameshift mutations that completely lack the second α/β motif and missense mutations that disrupt the interaction between the two motifs (Fig. 1f and Supplementary Table 2).

Another unique feature of the fingers domain is that it contains two nuclear localization signals (NLS1 and NLS2), which play a redundant role in targeting menin to the nucleus (Supplementary Fig. 3a) (Guru et al., 1998). NLS1 (amino acids 479-497), in the middle of the predicted unstructured loop, is not included in the current menin structure (Fig. 1c). In contrast, NLS2 is at the C-terminus of the protein (Fig. 1c), and part of it folds into a short α helix (α22) that protrudes away from the rest of the protein and binds to a neighboring molecule in the crystals (Supplementary Fig. 4j). The helical structure of NLS2 seen here is very different from the extended-chain conformation adopted by NLS peptides when bound to their associating proteins that impose a particular conformation on the NLS peptides[11]. As signals for subcellular localization are in general short peptide segments and recognized by their linear sequence, we expect that the menin NLS2 will be an extended chain, not an α helix, when bound to importin molecules. The propensity of NLS2 to form an α helix, however, might also confer this region of menin additional functions after menin is translocated into the nucleus. Further investigation is needed to clarify this possibility.

In addition to NLS1 and NLS2, we previously identified an accessory NLS (NLSa) (residues 546-572) in menin . Notably, NLSa folds into two short α helices and mediates the association between the two α/β motifs in the fingers domain (Supplementary Fig. 4i). Thus, consistent with its name, NLSa only plays an accessory role as a nuclear localization signal[12].

Supplementary References

1. Chandrasekharappa, S. C. et al. Positional cloning of the gene for multiple endocrine neoplasia-type 1. *Science* **276**, 404-7 (1997).
2. Prilusky, J. et al. FoldIndex: a simple tool to predict whether a given protein sequence is intrinsically unfolded. *Bioinformatics* **21**, 3435-8 (2005).
3. Holm, L. & Rosenstrom, P. Dali server: conservation mapping in 3D. *Nucleic Acids Res* **38**, W545-9.
4. Makarova, K. S., Aravind, L. & Koonin, E. V. A superfamily of archaeal, bacterial, and eukaryotic proteins homologous to animal transglutaminases. *Protein Sci* **8**, 1714-9 (1999).
5. Lee, J. H., Choi, J. M., Lee, C., Yi, K. J. & Cho, Y. Structure of a peptide:N-glycanase-Rad23 complex: insight into the deglycosylation for denatured glycoproteins. *Proc Natl Acad Sci U S A* **102**, 9144-9 (2005).
6. Lamb, J. R., Tugendreich, S. & Hieter, P. Tetratrico peptide repeat interactions: to TPR or not to TPR? *Trends Biochem Sci* **20**, 257-9 (1995).
7. Heery, D. M., Kalkhoven, E., Hoare, S. & Parker, M. G. A signature motif in transcriptional co-activators mediates binding to nuclear receptors. *Nature* **387**, 733-6 (1997).
8. Dreijerink, K. M. et al. Menin links estrogen receptor activation to histone H3K4 trimethylation. *Cancer Res* **66**, 4929-35 (2006).

9. Scheufler, C. et al. Structure of TPR domain-peptide complexes: critical elements in the assembly of the Hsp70-Hsp90 multichaperone machine. *Cell* **101**, 199-210 (2000).

10. Ikegami, T. et al. Solution structure of the DNA- and RPA-binding domain of the human repair factor XPA. *Nat Struct Biol* **5**, 701-6 (1998).

11. Cook, A., Bono, F., Jinek, M. & Conti, E. Structural biology of nucleocytoplasmic transport. *Annu Rev Biochem* **76**, 647-71 (2007).

12. La, P. et al. Tumor suppressor menin: the essential role of nuclear localization signal domains in coordinating gene expression. *Oncogene* **25**, 3537-46 (2006).

Supplementary Table 1 | Data Collection, Phasing, and Refinement Statistics

	Se-Met Menin-MLL1$_{MBM}$		Menin	Menin -MLL1$_{MBM}$	Menin-MLL1 -LEDGF$_{IBD}$	Menin -JunD$_{MBM}$
Data collection						
Data Set	Peak	Inflection				
Space group	*P4$_1$2$_1$2*	*P4$_1$2$_1$2*	*P4$_1$*	*P4$_1$2$_1$2*	*P6$_1$22*	*P4$_1$2$_1$2*
Cell dimensions						
a = *b* (Å)	140.537	140.758	139.891	141.205	187.953	140.637
c (Å)	90.501	90.250	54.146	93.550	238.417	93.069
-α, β, γ (°)	90, 90, 90	90, 90, 90	90, 90, 90	90, 90, 90	90, 90, 120	90, 90, 90
Wavelength (Å)	0.97940	0.97955	1.07819	0.97941	0.97872	0.98019
Resolution (Å)*	100-3.00 (3.11-3.00)	100-3.23 (3.38-3.23)	100-2.5 (2.59-2.50)	100-3.0 (3.11-3.00)	100-2.8 (2.90-2.80)	100-2.65 (2.70-2.65)
R_{merge} (%)*	11.9 (55.3)	11.1 (63.5)	9.6 (46.5)	8.8 (33.4)	12.9 (70.5)	10.6 (65.3)
I / □	31.8 (2.6)	25.5 (3.7)	23.1 (4.1)	40.9 (9.4)	26.2 (2.3)	23.9 (2.4)
Completeness (%)*	81.4 (56.0)	81.9 (65.9)	100 (100)	94.6 (75.5)	99.5 (96.2)	92.0 (72.6)
Redundancy*	30.8 (12.5)	22.3 (14.9)	7.0 (5.5)	23.7 (20.4)	13.9 (5.8)	11.5 (6.2)
Refinement						
Resolution (Å)			50-2.5	40-3.0	48.6-2.8	34-2.66
No. of reflections			36690	18442	61099	25134
R_{work} / R_{free} (%)			19.63/24.05	23.05/26.54	21.20/25.32	22.73/27.87
Number of atoms						
-Proteins			7760	3900	9815	3931
-Water			50			12
B-factors						
-protein			48.184	116.315	76.884	90.033
-water			41.773			68.459
Rms deviations						
-Bond lengths (Å)			0.0063	0.0075	0.009	0.009
-Bond angles (°)			1.2481	1.3711	1.376	1.291

Supplementary Table 2 | Structural analysis of the MEN1-related missense mutations and in-frame deletions.

Residue No.	WT	Mutant	Domain	Conserved (Yes or No)	Exposed or Internal	Defects inside	Clinical symptoms*
12	P	L	NTD	Y	E		
22	L	R	NTD	Y	I	α1-α4 helix bundles	PanNET
37	L	P	NTD	Y	I	α1-α4 helix bundles	
39	L	W	NTD	Y	I	α1-α4 helix bundles	HPT, PET and PIT
42	G	S	NTD	Y	I	α1-α4 helix bundles	
42	G	D	NTD	Y	I	α1-α4 helix bundles	HPT, PET and PIT
43	FV	L	NTD	Y	I	α1-α4 helix bundles	HPT, PET and PIT
45	E	G	NTD	Y	I	interface of NTD and Thumb	HPT and NET-meta
45	E	D	NTD	Y	I	interface of NTD and Thumb	
49	A	P	NTD	N	I	interface of NTD, Thumb and Palm	
53	V	I	NTD	N	E		
86	I	F	NTD	N	I	α1-α4 helix bundles	
89	L	R	NTD	Y	I	interface of NTD and Thumb	
119	K	deletion	Thumb	Y	E		HPT and PET
120	K	deletion	Thumb	Y	E		HPT and PIT
126	W	G	Thumb	Y	I		
139	H	D	Thumb	Y	I	MLL-binding	
139	H	Y	Thumb	Y	I	MLL-binding	
139	H	R	Thumb	Y	I	MLL-binding	
144	F	V	Thumb	Y	I	interfaceof NTD and Thumb	
144	F	C	Thumb	Y	I	interface of NTD and Thumb	HPT
156	G	D	Thumb	Y	I	MLL-binding	
159	F	C	Thumb	N	I	MLL-binding	
160	A	T	Thumb	Y	I	interface of α5 and α7	
160	A	P	Thumb	Y	I	interface of α5 and α7	HPT, PET and PIT
162	V	F	Thumb	Y	I	interface of NTD, Thumb and Palm	HPT and PET
164	A	D	Thumb	Y	I	interface of α5 and α7	HPT and PET
164	A	V	Thumb	Y	I	interface of α5 and α7	PanNET
165	C	R	Thumb	Y	I	interface of α5 and α7	ADR, HPT, PET, PIT
171	R	Q	Thumb	N	E		
172	D	Y	Thumb	Y	I		HPT, PET , PIT HPT and PET-meta HPT, PET-meta, PIT HPT, PET-ZES,PIT
172	D	V	Thumb	Y	I		
175	L	R	Thumb	Y	I	MLL-binding	
176	A	P	Thumb	Y	I	MLL-binding	
178	S	Y	Thumb	Y	I	MLL-binding	
179	E	D	Thumb	Y	I	MLL-binding	ADR, HPT, PET, PIT
183	W	S	Thumb	Y	I	MLL-binding	ADR, HPT, PET, PIT
183	W	R	Thumb	Y	I	MLL-binding	PanNET
184	V	E	Thumb	Y	I	α/β interface of Thumb	HPT
197	T	deletion	Thumb	Y	I	α/β interface of Thumb	HPT, NET-meta, PET, PIT
225	G	V	Thumb	Y	E		PanNET
241	C	R	Palm	N	I	MLL-binding	
241	C	F	Palm	N	I	MLL-binding	HPT
242	A	V	Palm	Y	I	MLL-binding	
255	E	K	Palm	Y	I	interface of NTD and Palm	HPT
260	Q	P	Palm	Y	E	Palm topology	HPT
264	L	P	Palm	Y	I	Palm topology	HPT, PET and PIT
267	L	P	Palm	Y	I	Palm topology	HPT
281	G	R	Palm	Y	I	MLL-binding	CNS, HPT and PIT
284	A	E	Palm	N	I	MLL-binding	HPT, PET and PIT
286	L	P	Palm	Y	I	Palm topology	
309	A	P	Palm	N	I	Palm topology	
311	T	P	Palm	N	E	Palm topology	HPT and PET
314	R	P	Palm	N	E	Palm topology	HPT and PET
317	H	Y	Palm	Y	I	interface of Thumb and Palm	ADR, HPT and PET
317	H	R	Palm	Y	I	interface of Thumb and Palm	HPT and NET
320	P	R	Palm	Y	I	MLL-binding	PanNET
337	A	D	Palm	Y	I	Palm topology	HPT and PET
340	A	T	Palm	N	I	Palm topology	
341	W	R	Palm	Y	I	Palm topology	ADR, HPT and PET
344	T	R	Palm	N	I	Palm topology	
357	D	H	Palm	Y	I	interface of Thumb and Palm	HPT
358	E	deletion	Palm	Y	E	MLL-binding	HPT and PET
363	E	deletion	Palm	Y	E	MLL-binding	
368	A	D	Palm	Y	I	interface of Palm and Fingers	HPT, PET-ZES, PIT
414	L	deletion	Fingers	Y	I	internal interface of Fingers	HPT
418	D	N	Fingers	Y	I	internal interface of Fingers	ADR and HPT HPT, PET and PIT
418	D	deletion	Fingers	Y	I	internal interface of Fingers	
425	E	deletion	Fingers	Y	E		ADR, CNS, HPT, PET-ZES and PIT
429	T	K	Fingers	Y	E		
436	W	R	Fingers	Y	I	interface of Palm and Fingers	
444	L	P	Fingers	N	I	internal interface of Fingers	HPT, PET and PIT
447	F	S	Fingers	Y	I	interface of Palm and Fingers	
552	T	S	Fingers	N	E		
555	S	N	Fingers	Y	I	internal interface of Fingers	HPT and PET
557	K	deletion	Fingers	Y	I	internal interface of Fingers	HPT, PET and PIT
237-239	AFM	deletion	Thumb	N	I	MLL-binding	HPT, PET and PIT
264-266	LWL	deletion	Thumb	Y	I	Palm topology	
418-422	DGICK	E	Fingers	Y	I	internal interface of Fingers	HPT, NET, PET, PIT, THYR
453-456	QKVR	deletion	Fingers	N	I	internal interface of Fingers	

*Abbreviations:

HPT, hyperparathyroidism; PET, endocrine pancreas tumors; PIT, anterior pituitary tumors; NET, thymic/bronchic neuroendocrine tissue tumors; ADR, adrenal gland tumors; PanNET, pancreatic neuroendocrine tumors; NET-meta, metastatic thymic/bronchic neuroendocrine tissue tumors; THYR, thyroid epithelioma; CNS, central nervous system tumors; PET-ZES, endocrine pancreas Zollinger-Ellison syndrome;

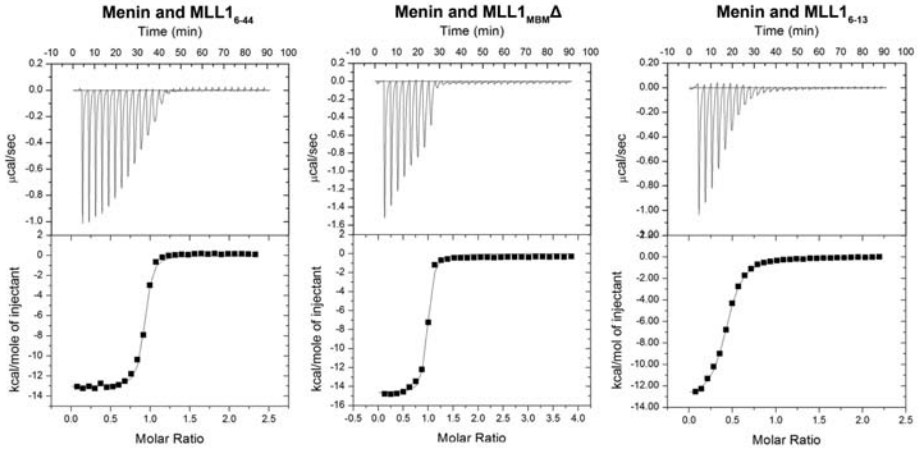

Supplementary Figure 1 | ITC Measurements of interaction between menin and various N-terminal fragments of MLL1 (related to Fig. 1a).

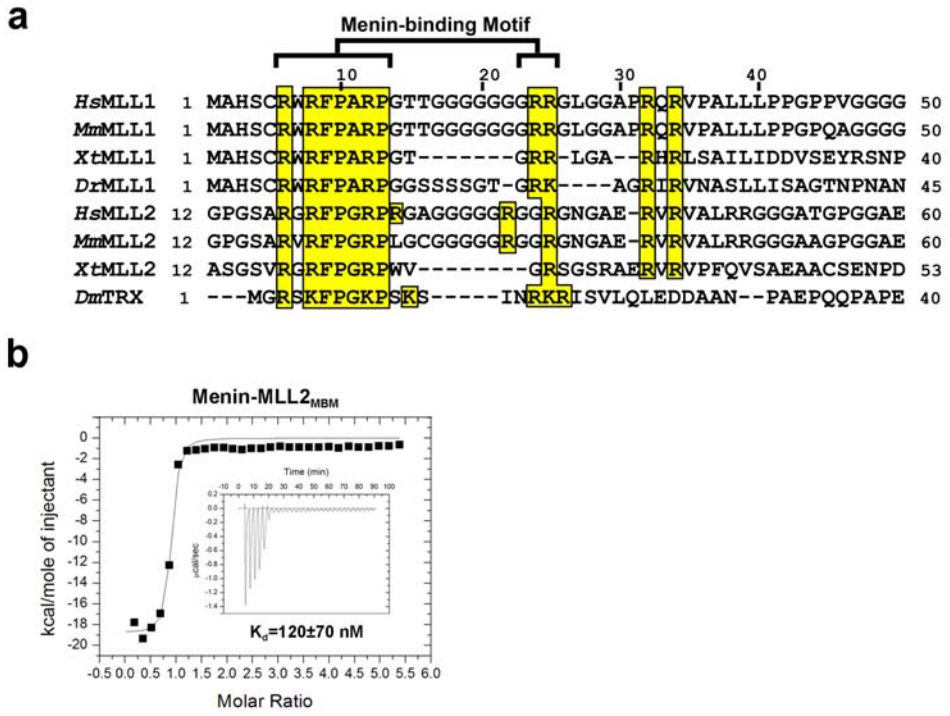

Supplementary Figure 2 | Characterization of the menin-MLL interaction. a, Sequence alignment of the extreme N-termini of MLL1, MLL2 and TRX proteins from different organisms (*Hs*: *Homo sapiens*; *Mm*: *Mus musculus*; *Xt*: *Xenopus tropicalis*; *Dr*: *Danio rerio*; *Dm*: *Drosophila melanogaster*). The conserved residues and the basic residues are highlighted in yellow boxes. **b,** ITC measurement of the interaction of menin with the $MLL2_{MBM}$ peptide. Insert is the ITC titration data. The binding curve was fit to a one-binding-site-per-menin model.

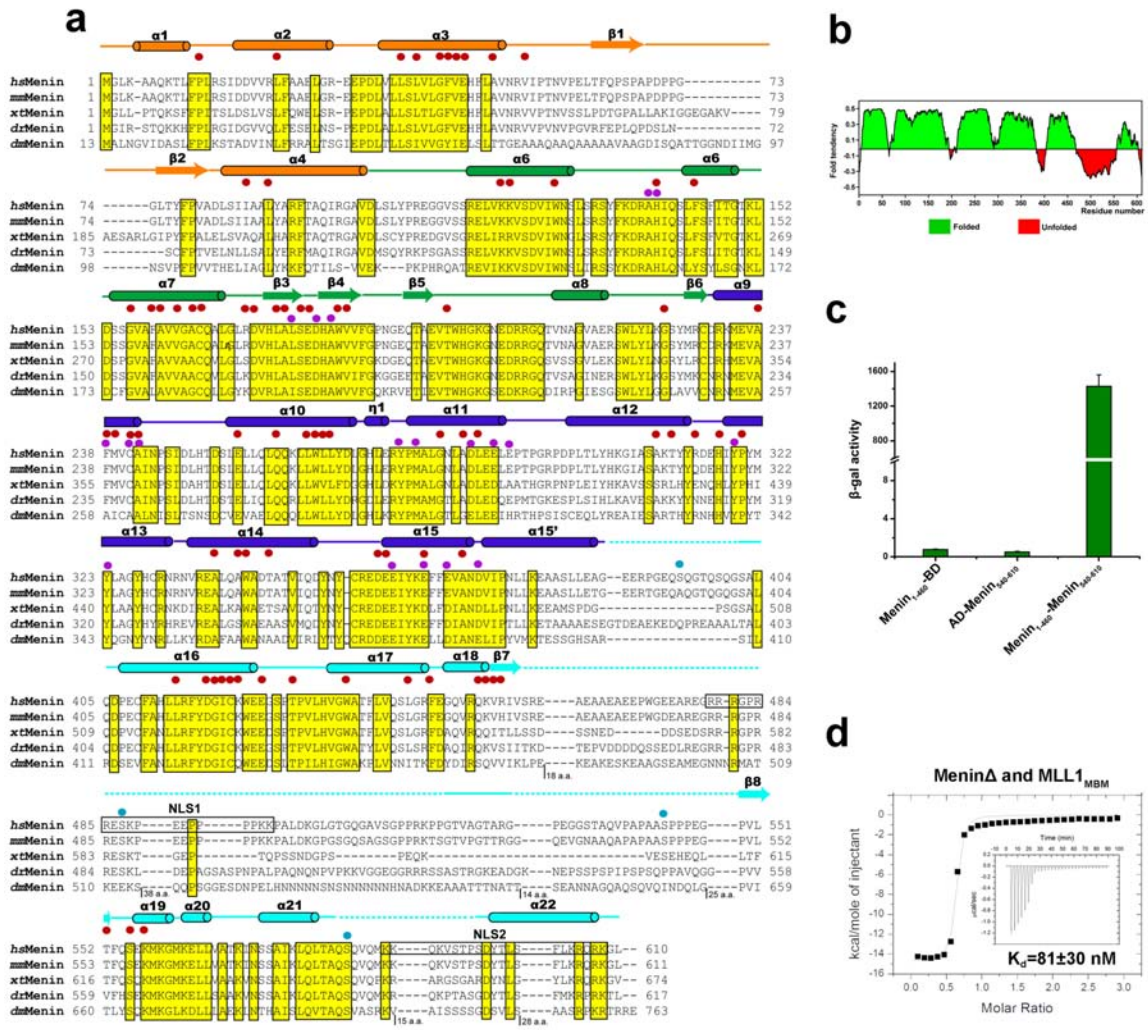

Supplementary Figure 3 | Crystallization of the Menin-MLL1$_{MBM}$ Complex. a, Primary sequence alignment of menin family members. Secondary structure assignments are shown as cylinders (α helices) and arrows (β strands), and colored as in Fig. 1c. Red dots denote MEN1-related missense mutations or in-frame deletions, purple dots denote residues involved in MLL1 binding, and cyan dots label the phosphorylation sites. Conserved residues are highlighted in yellow. Nuclear localization sequences (NLS) are boxed. **b,** Protein folding analysis of menin by FoldIndex program. **c,** Interaction between Menin$_{1-460}$ and Menin$_{540-610}$, detected by yeast-two-hybrid. **d,** ITC measurement of the interaction of menin$_{\Delta 460-519}$ with the MLL1$_{MBM}$ peptide.

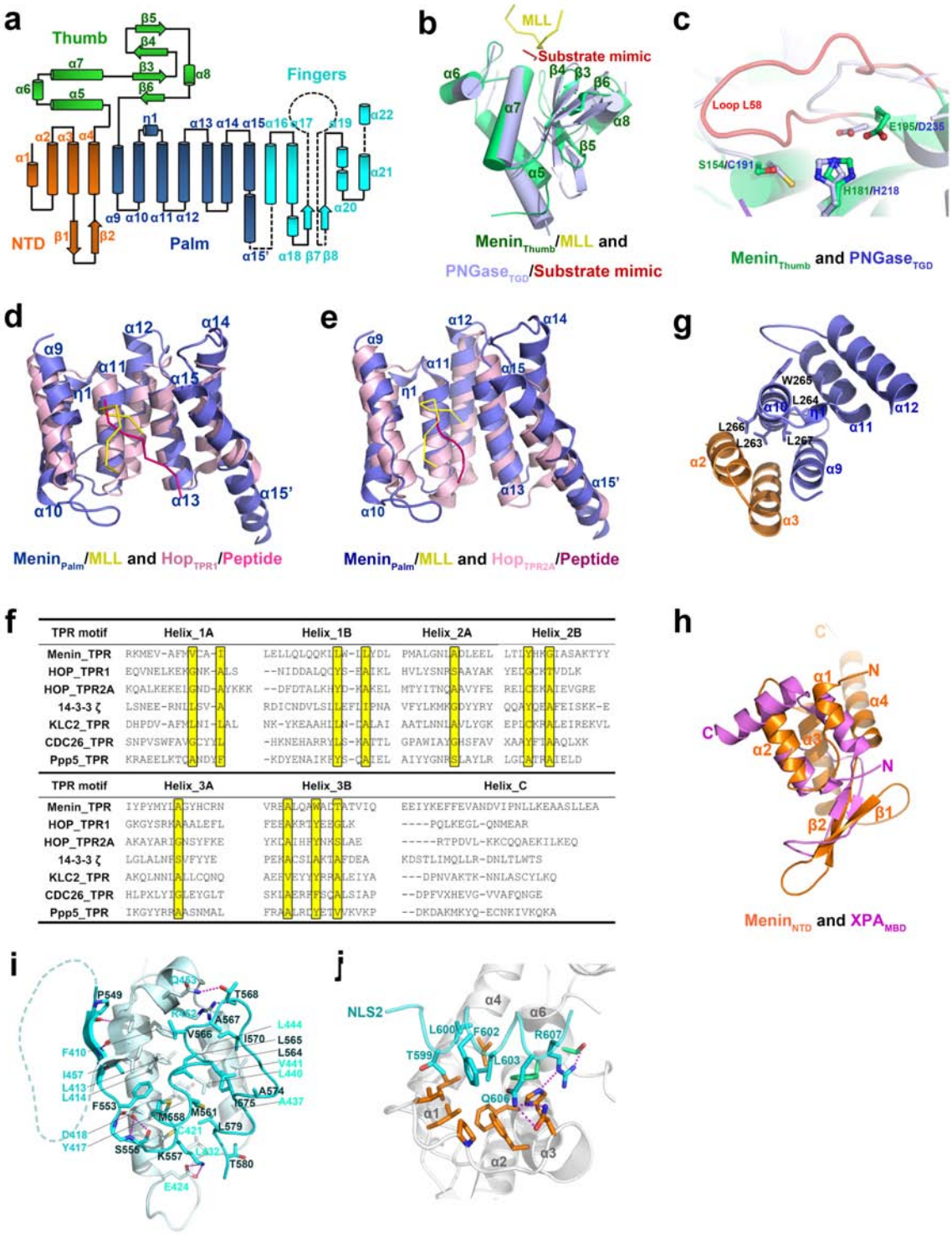

Supplementary Figure 4 | Structural architecture of menin. a, The topology diagram of menin that is colored as in Fig. 1c. **b,** Superposition of the structure of Menin$_{thumb}$-MLL1$_{MBM}$ on that of human PNGase$_{TGD}$-substrate mimic. Menin$_{Thumb}$-MLL1$_{MBM}$ and PNGase$_{TGD}$-substrate mimic are colored in green and yellow,

and light-blue and red, respectively. **c,** Structural alignment of $Menin_{Thumb}$ and $PNGase_{TGD}$ that shows the superposed catalytic triad as well as the loop L58 that buries the triad in menin structure. **d,** Structural alignment between the $menin_{palm}$-$MLL1_{MBM}$ and the Hop_{TPR1}-peptide complexes. $menin_{palm}$-$MLL1_{MBM}$ and Hop_{TPR1}-peptide are colored in blue and yellow, and pink and magenta, respectively. **e,** Structural superposition between the complexes $menin_{Palm}$-$MLL1_{MBM}$ and Hop_{TPR2A}/peptide. $menin_{Palm}$-$MLL1_{MBM}$ and Hop_{TPR2A}-peptide are colored in blue-yellow and pink-magenta, respectively. **f,** Structure-based sequence alignment of the TPR domains among menin and other TPR-containing proteins. The TPR consensus residues are highlighted in yellow. **g,** The LLWLL motif of menin is located within a buried environment. **h,** Superposition of $menin_{NTD}$ (orange) and XPA_{MBD} (pink) highlights the common β-sheet and the α1 and α2 helices. **i,** Interactions between the two α/β motifs in the fingers domain of menin. The two α/β motifs are colored in palecyan and teal, respectively. Interacting residues of the two motifs are represented as stick models, and hydrogen bonds are denoted as magenta dash lines. **j,** NLS2 adopts a helical conformation and binds to a neighboring molecule in the crystal. NLS2 is colored cyan, and the interacting residues in the other molecule are colored orange (NTD) or green (Thumb domain).

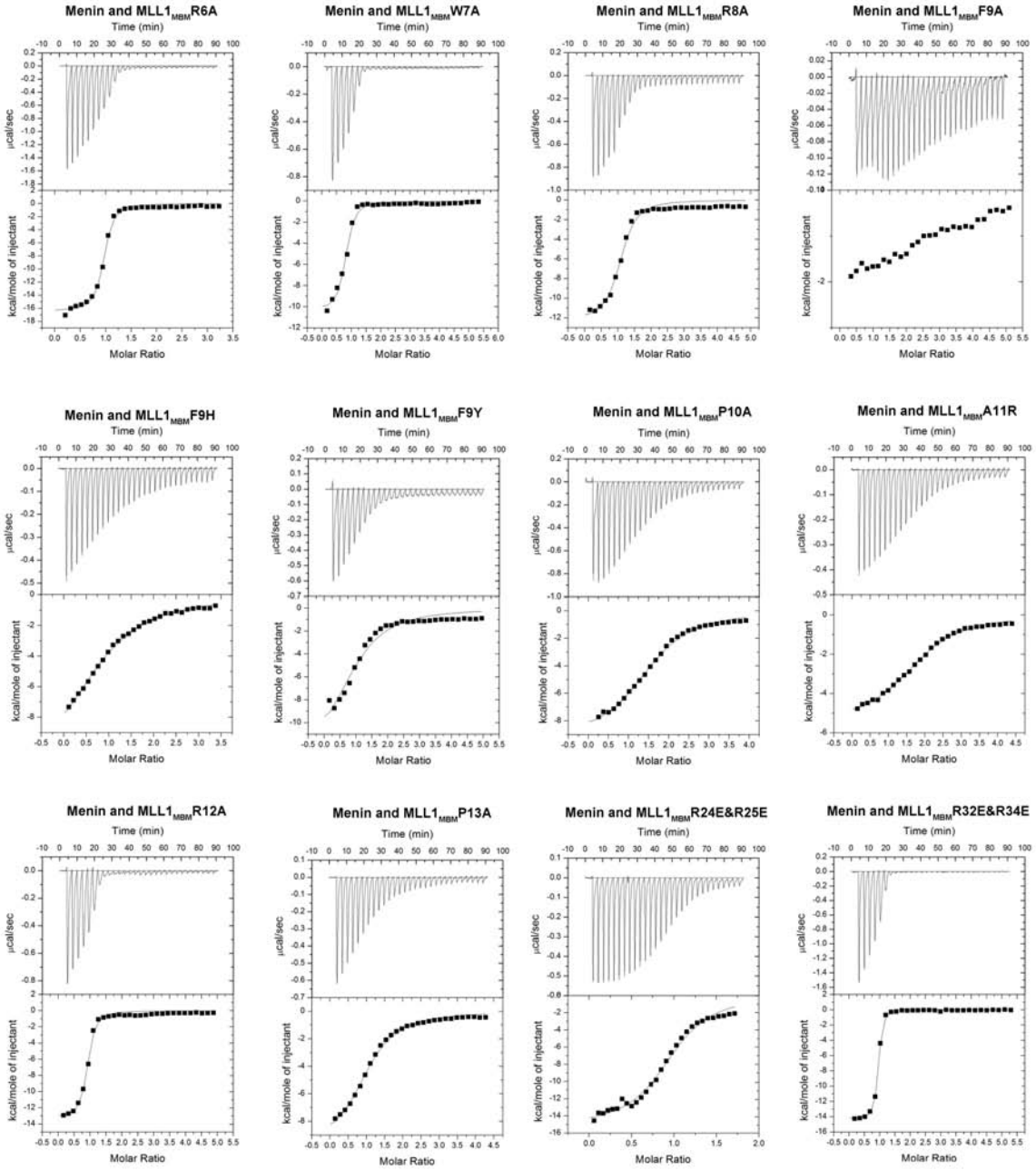

Supplementary Figure 5 | ITC measurements of interaction between menin and $MLL1_{MBM}$ mutants (related to Fig. 2b).

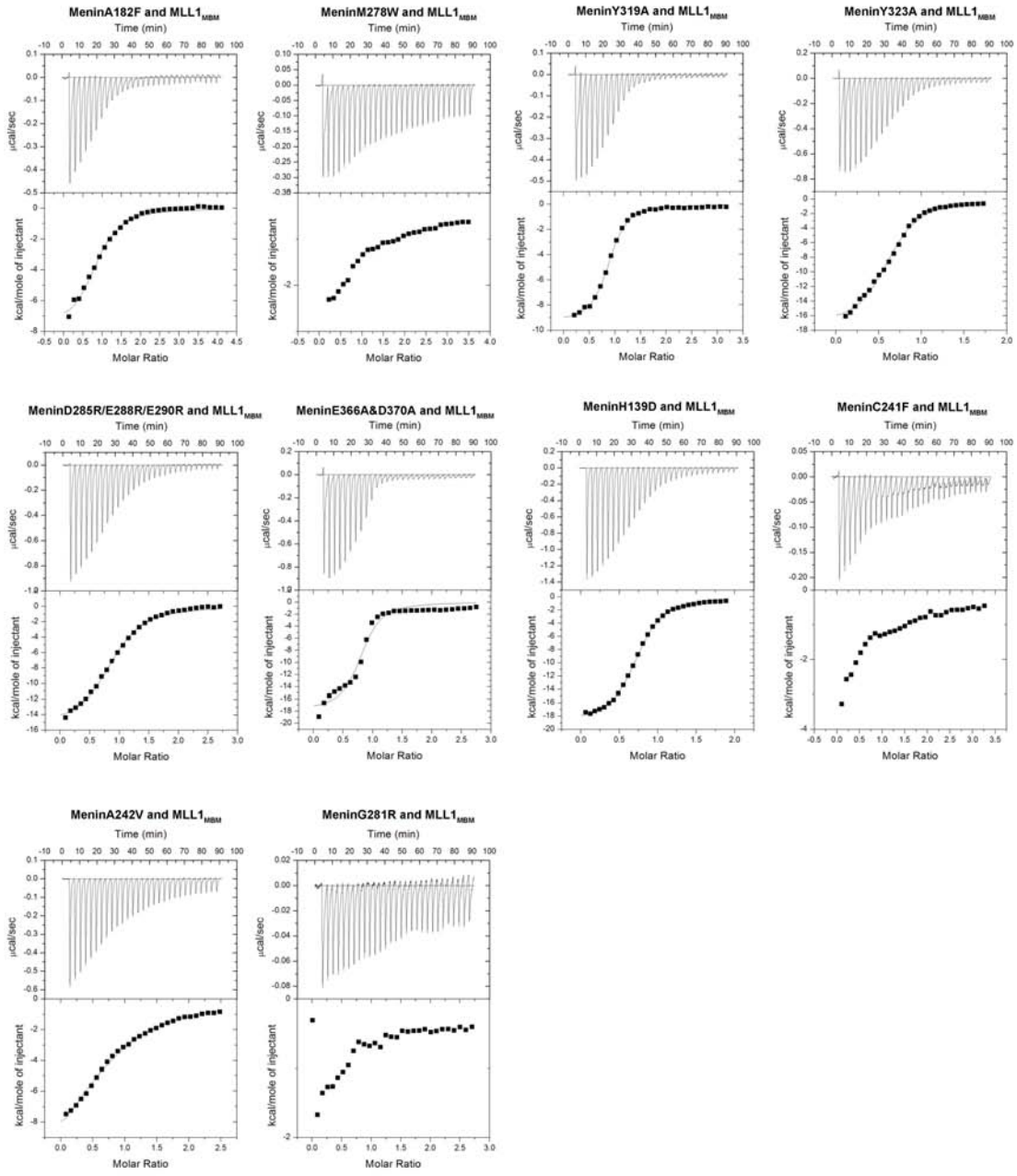

Supplementary Figure 6 | ITC measurements of interaction between $MLL1_{MBM}$ and menin mutants (related to Fig. 2c).

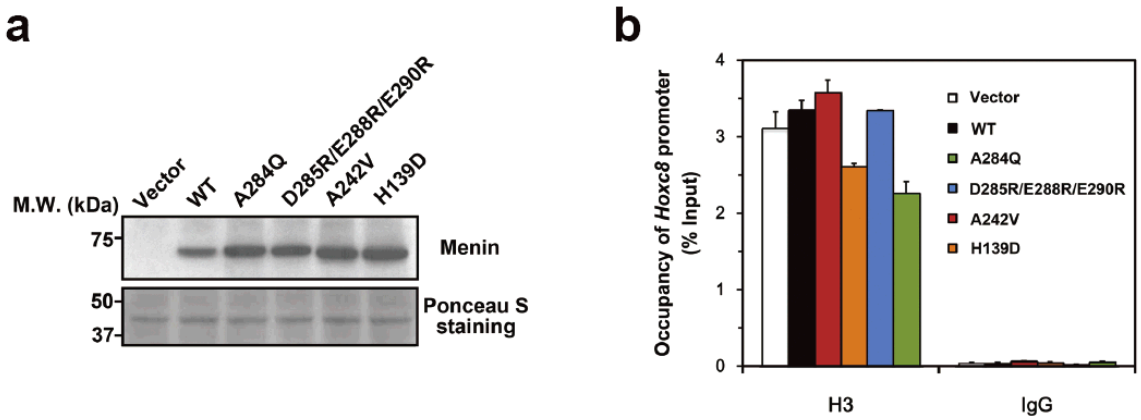

Supplementary Figure 7 | In vivo functional analysis of the menin-MLL1 interaction. **a,** Expression level of wild-type and mutant menin detected by western blot, related to Figs. 2h-2j. **b,** Expression of wild-type and mutant menin in menin-null MEFs does not significantly affect histone H3 distribution at the *Hoxc8* promoter region.

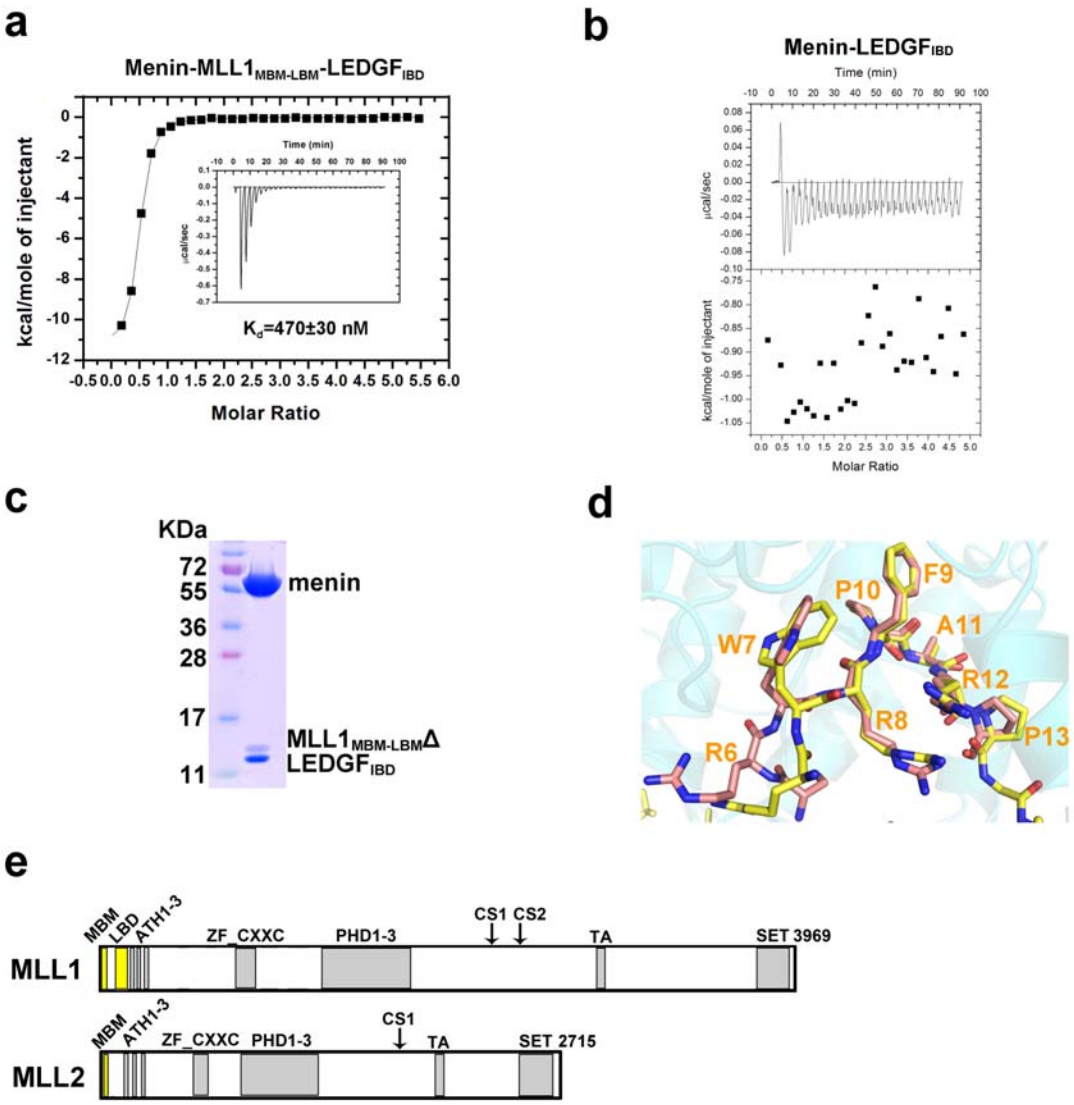

Supplementary Figure 8 | Characterization of the interaction between LEDGF and the menin-MLL1 complex. a, ITC measurement of the interaction between $LEDGF_{IBD}$ and the menin-$MLL1_{MBM-LBM}$ complex. **b,** ITC measurement of the interaction between $LEDGF_{IBD}$ and menin. We could not perform the ITC measurement of the interaction between $LEDGF_{IBD}$ and $MLL1_{MBM-LBM}$, as the $MLL1_{MBM-LBM}$ peptide is prone to be degraded by itself. We tried the co-expression and co-purification of $LEDGF_{IBD}$ and $MLL1_{MBM-LBM}$, but could not get the protein complex (data not shown). **c,** $MLL1_{MBM-LBM}\Delta$ could form a stable protein complex with menin and $LEDGF_{IBD}$, as shown in the SDS-PAGE. The staining difference between $MLL1_{MBM-LBM}\Delta$ and $LEDGF_{IBD}$ results from the composition difference of basic residues. **d,** Comparison of $MLL1_{MBM}$ in the structures of menin-$MLL1_{MBM}$ (red) and menin-$MLL1_{MBM-LBM}\Delta$-$LEDGF_{IBD}$ (yellow). **e,** Comparison of the domain organizations between MLL1 and MLL2. MLL2 lacks an LBM fragment.

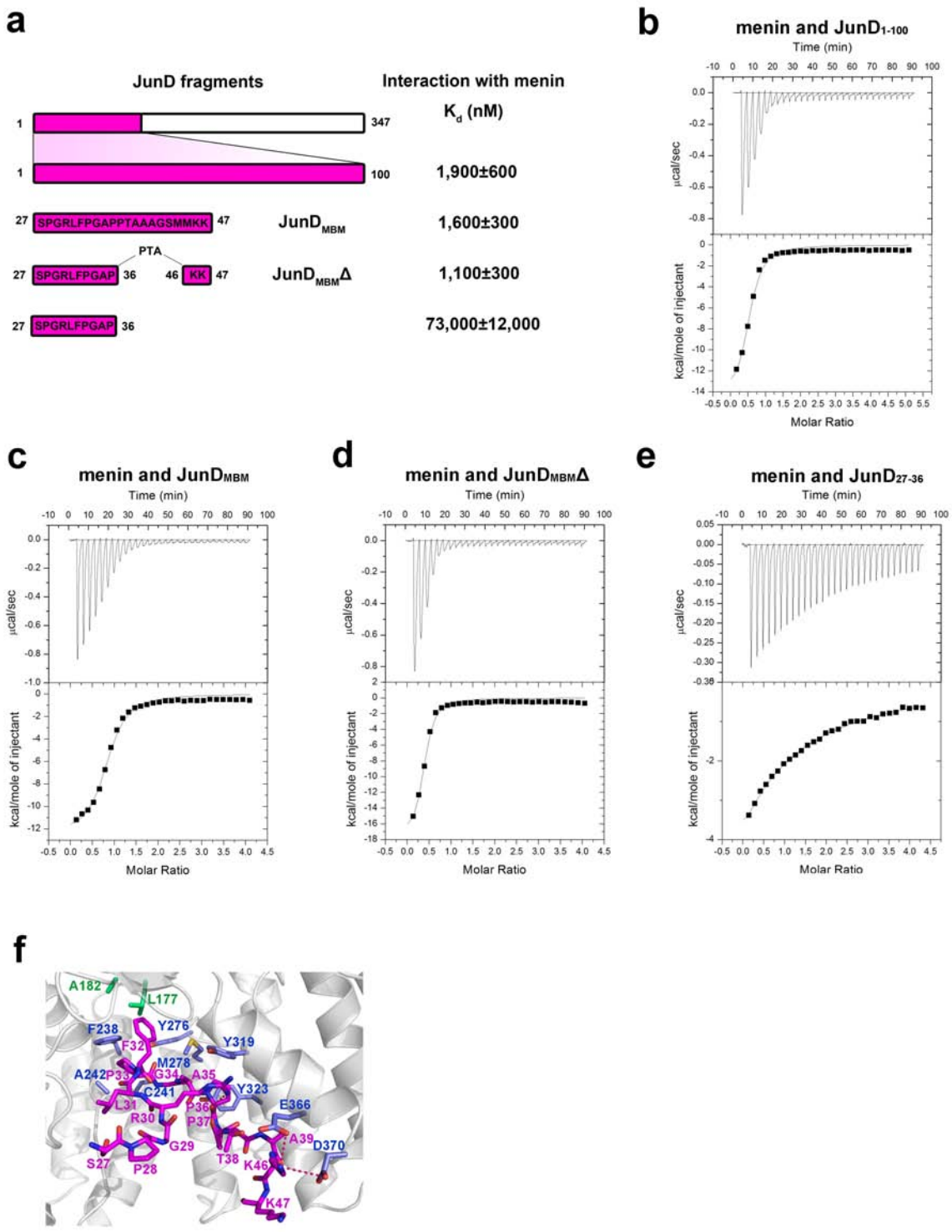

Supplementary Figure 9 | Characterization of the interaction between menin and $JunD_{MBM}$. a, Summary of ITC analysis of the interaction between menin and various JunD peptides. **b,** ITC measurement of the interaction between menin and $JunD_{1-100}$. **c,** ITC measurement of the interaction between menin and $JunD_{MBM}$. **d,** ITC measurement

of the interaction between menin and $JunD_{MBM}\Delta$. **e,** ITC measurement of the interaction between menin and $JunD_{27\text{-}36}$. **f,** The menin-$JunD_{MBM}$ interface. $JunD_{MBM}$ (magenta) and the interacting residues in menin (green: residues in the thumb domain; blue: residues in the palm domain) are presented as stick models. The Menin-$JunD_{MBM}$ intermolecular hydrogen bonds are shown as pink dash lines.

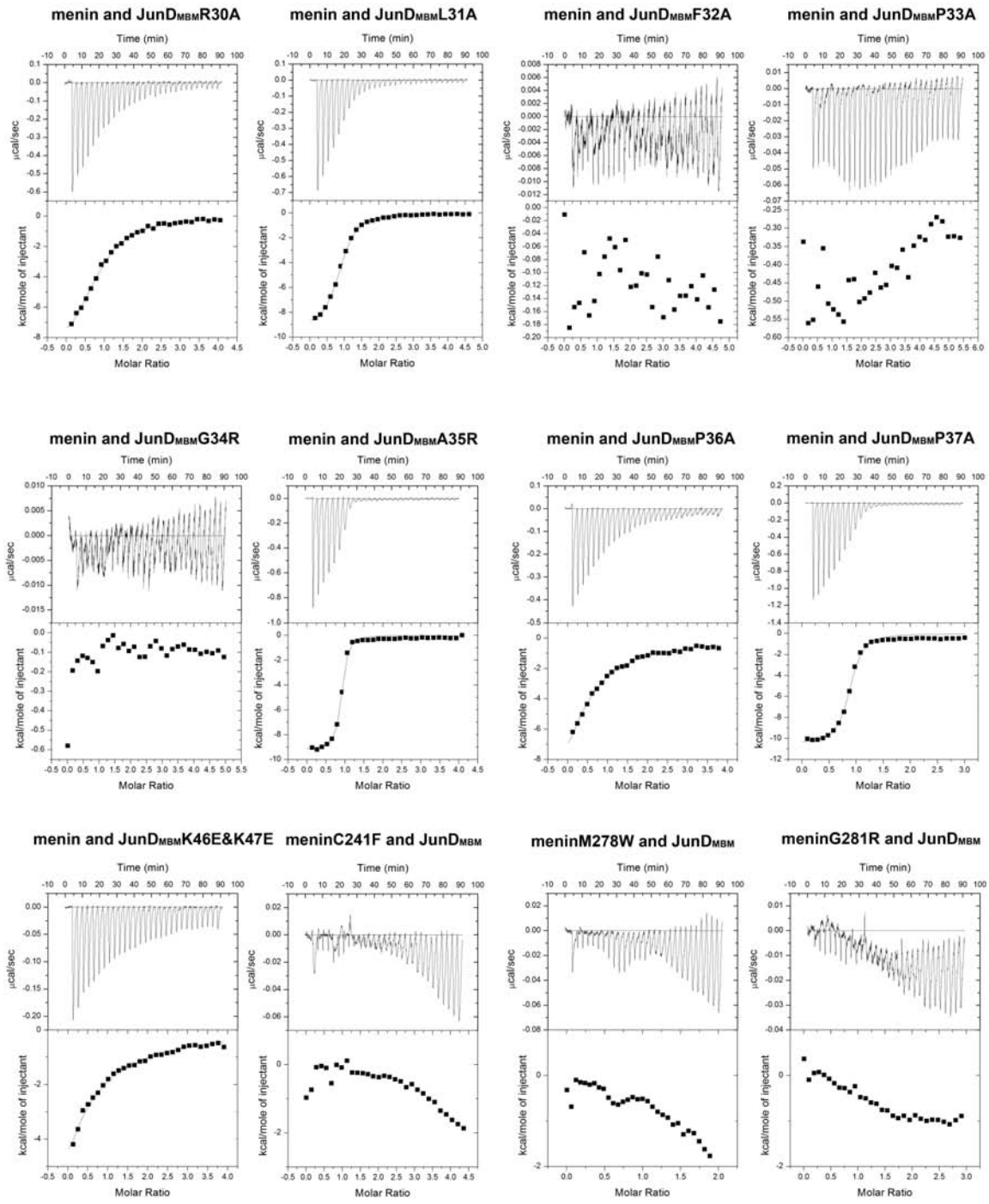

Supplementary Figure 10 | ITC measurements of interactions between menin and $JunD_{MBM}$ mutants (related to Fig. 4d).

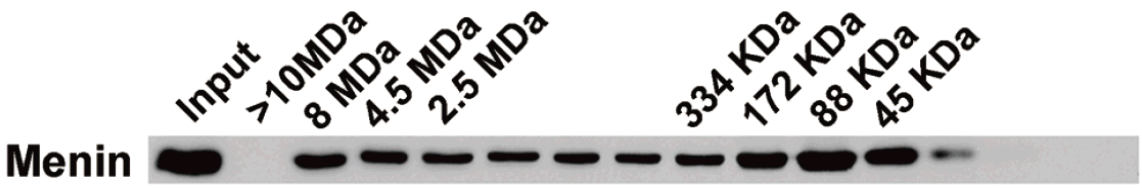

Supplementary Figure 11 | Immunoblot analysis of endogenous menin following fractionation on a Superpose 6 gel-filtration column. Positions of molecular weight markers are indicated.